SDHT for Fast Detection of Weak GNSS Signals

Seung-Hyun Kong, *Member, IEEE*

***Abstract*—Successful and fast Global Navigation Satellite System (GNSS) positioning in indoor environments can enable many location based services (LBS). However, fast indoor GNSS positioning has been one of the biggest challenges for GNSS receivers due to the huge computational cost. To detect weak GNSS signals in indoor environments, a GNSS receiver should perform numerous correlations with a longer coherent integration interval for a denser Doppler frequency search, which is computationally too expensive. For a fast and low computational weak GNSS signal detection, we propose the synthesized Doppler frequency hypothesis testing (SDHT) technique that, utilizing the test results of only sparse Doppler frequency hypotheses, can estimate the test results of entire Doppler frequency hypotheses with small computations. We provide theoretical performance analysis of the proposed technique and demonstrate that the proposed technique reduces the computational cost for weak GNSS signal acquisition significantly and achieves faster signal acquisition than conventional techniques.**

***Index Terms*—Indoor GNSS, low computational detection, sensitivity enhancement, Doppler frequency.**

I. Introduction

THE acquisition of an incoming Global Navigation Satellite System (GNSS) signal requires numerous tests of the code phase and Doppler frequency hypotheses [1]. A hypothesis testing is performed by a correlation and integration, and the total number of code phase hypotheses and that of Doppler frequency hypotheses depend on the code length of spreading sequence and the coherent integration interval T, respectively. Since the code length is a multiple of $L_c(=1023)$ chips in GNSS, and the Doppler frequency of a GNSS signal is between -5 kHz and $+5$ kHz, the number of total hypotheses can be a multiple of $2L_c\lceil 2\times 10^4 T+1\rceil$. For example, for legacy Global Positioning System (GPS) receivers using $T=10^{-3}$s the number of total hypotheses to test is $42L_c$ so that it takes $42L_cT$ seconds for a receiver to test all the hypotheses serially with a single correlator. Therefore, for a fast signal acquisition GNSS receivers may need a large number of parallel correlators, which, in general, increases the hardware complexity of receivers.

Alternatively, a GNSS receiver may be equipped with a digital signal processor (DSP) that computes $\mathbf{Y}$ and $\mathbf{X}$, the Fast Fourier Transforms (FFT) of the incoming GNSS signal samples and receiver generated replica signal for a Doppler frequency hypothesis to test, respectively, and performs an inner-product (i.e., $\mathbf{Y}\cdot\mathbf{X}^*$) and an inverse FFT (IFFT) of $\mathbf{Y}\cdot\mathbf{X}^*$ to obtain auto-correlation function (ACF) output at all code phases for a Doppler frequency hypothesis being tested, where $(\cdot)$ and $()^*$ represent the inner-product and the complex conjugate operation, respectively. This FFT-based technique [2] is widely used recently as DSP becomes cheaper. To reduce the computational complexity of the FFT-based technique, there have been a number of studies introduced in the literature. Averaging correlator (AC) technique [3] is a useful fast FFT-based technique when the sampling rate is much larger than the chip-rate, shifting replica (SR) technique [4] circularly shifts the components of $\mathbf{Y}$ to obtain $\mathbf{Y}'$ and computes IFFT of $\mathbf{Y}'\cdot\mathbf{X}^*$ to find ACF outputs for a Doppler frequency at $1/T$Hz apart from the previously tested Doppler frequency, and block averaging pre-processing (BAP) technique [5] reduces computational cost for long coherent integration by applying FFT operation to the 1 ms signal sample block that is made of Doppler frequency compensated incoming GNSS signal samples averaged over multiple 1 ms blocks. The BAP and the fast BAP techniques require only 50% and 10% of the conventional FFT-based technique for weak and strong GNSS signal detection, respectively; however, the 10 times lower computations with the fast BAP technique renders strong noise amplification and limited application of the technique only to strong signals. Recent folding techniques [6] and [7] and FFT-based two-dimensional compressed correlator (TDCC) technique [8] achieve fast acquisition with low computational cost, however, these techniques suffer from SNR loss more or less as the folding number and compression rate increases, respectively.

Other techniques enhance the sensitivity of GNSS receivers at the cost of additional hardware. A-GPS (Assisted-GPS) technique [9] and [10] utilizes a prompt wireless connection to a GPS-synchronized base station to receive fine timing and frequency assistance, and hybrid GPS receiver [11] makes use of wireless connection to other nodes and inertial measurement unit (IMU) to lower the computational complexity in long coherent integration. Recent multi-satellite maximum likelihood (MSML) acquisition technique [12] can reduce the computational cost for the simultaneous acquisition of multiple satellites in A-GPS [9], where the detection sensitivity improvement is from compensating the interference to weak signals from strong satellites.

To detect weak GNSS signals (for example, $\mathrm{C/N_0} <$ 30 dB-Hz), a standalone GNSS receiver may either perform a coherent integration with long coherent interval $T(\gg 1$ ms) or a non-coherent accumulation of multiple ($N_{nc}\gg 1$) coherent integration outputs with a short coherent integration interval T_{co}. In practice, however, both are computationally expensive;

Manuscript received June 12, 2014; revised November 27, 2014; accepted January 6, 2015. Date of publication May 6, 2015; date of current version October 19, 2015. This work (2013R1A2A2A01067863) was supported by Mid-career Researcher Program through NRF grant funded by the Korean government (MEST).

The author is with CCS Graduate School for Green Transportation, Korea Advanced Institute of Science and Technology (KAIST), Daejeon 305-701, Korea (e-mail: skong@kaist.ac.kr).

Color versions of one or more of the figures in this paper are available online at http://ieeexplore.ieee.org.

Digital Object Identifier 10.1109/JSAC.2015.2430291

the longer coherent integration interval T causes larger number of Doppler frequency hypotheses to test because of the smaller Doppler frequency search step size $\Delta_f \simeq \frac{1}{2T}$ and requires additional computations for bit transitions [13]. On the other hand, the non-coherent accumulation scheme renders overall integration interval $N_{nc}T_{co}$ much longer than T to compensate the large squaring loss [9]. Therefore, the increase of computational cost in the weak GNSS signal detection is inevitable.

In this paper, we investigate the problem of reducing the computational cost for the FFT-based parallel correlation technique using long coherent integration interval T. We propose the synthesized Doppler frequency hypothesis testing (SDHT) technique that, utilizing the test results of a subset of all Doppler frequency hypotheses, can estimate the test results of entire Doppler frequency hypotheses with low computations. For example, a GNSS receiver may perform FFT-based parallel code phase search for Doppler frequency hypotheses at $\frac{1}{2T_1}$ apart with a coherent integration interval $T_1(=1)$ms for $R_T(\gg 1)$ successive times, and the results can be utilized to estimate the FFT-based parallel code phase search for all other Doppler frequency hypotheses at $\frac{1}{2R_TT_1}$ apart with low computational cost. We provide the theoretical performance analysis of the proposed technique and performance comparison with other techniques to show the advantage of the proposed technique. It is demonstrated that the proposed technique reduces the computational cost of weak GNSS signal acquisition significantly and achieves faster signal acquisition than the conventional techniques.

The rest of this paper is organized as follows. In Section II, we analyze the complexity in detecting weak GNSS signals. In Section III, we introduce the component algorithms used for the proposed technique. Section IV provides in-detail realization of the proposed technique, and Section V shows the analysis of the performance and mean acquisition computation (MAC) of the proposed technique. The advantage of the proposed technique in comparison to other techniques is demonstrated using numerous Monte Carlo simulation results in Section VI, and, finally, Section VII concludes this paper.

Throughout this paper, following conventions are used for notations. Vectors or matrices are denoted by boldface symbols. Small letters are used for scalars and vectors, and capital letters are used for matrices and FFT output. Some of the key variables used in this paper are listed with definitions in Table II in Appendix C.

II. Complexity in Weak Signal Detection

In this paper, among various GNSS signals, we use BPSK modulated $L1$ frequency GPS coarse/acquisition (C/A) code signal to explain the proposed technique as one of the most widely used GNSS signals. However, the principle of the proposed technique is directly applicable to BOC signals.

Let $y(t)$ represent incoming GPS satellite signals that are down-converted to an IF frequency f_I as

$$y(t) = \sum_{k=1}^{K} A^k D^k(t-\tau_k) P^k(t-\tau_k) e^{j(2\pi(f_I+f_D^k)t+\theta_k)} + v(t), \quad (1)$$

where A^k, τ_k, f_D^k, and θ_k represent the amplitude, code phase, Doppler frequency, and unknown carrier phase of the k-th GPS signal, respectively, and $D^k(t)$, $P^k(t)$, $v(t)$ are the GPS navigation data with bit duration $T_b(=20$ ms), pseudo-random noise (PRN) sequence signal with code length $L_c(=1023)$ chips and code period $T_1(=1$ ms) (i.e., chip rate $R_c = 1.023$ MHz), and complex Gaussian noise with two-sided power spectral density (PSD) $N_0/2$, respectively. In general, $|f_D^k| \le 5$ kHz, and $D^k(t)$ can be assumed a constant during T for $T < T_b$. The IF signal $y(t)$ passes through a bandpass filter whose center frequency is at f_I with a bandwidth $B \ge 2R_c$.

To detect weak GNSS signals, higher sampling rate $f_s(\gg 2R_c)$ and longer correlation length $T(\gg T_b)$ are two of the most preferred choices for GNSS receivers. However, when T is large (i.e., $T \gg T_b$), the number of Doppler frequency hypotheses to test should be large, and $D^k(t)$ cannot be assumed constant during T so that the resulting ACF output is a function of code phase, Doppler frequency, and navigation data. Let $T = R_TT_1$ and R_T be an integer power of 2. To detect the weak signal $y(t)$ from an auto-correlation function (ACF) output, the receiver generates a receiver replica signal

$$x(t) = D_i(t-\tau_p-t_b)P(t-\tau_p)e^{j(2\pi(f_I+f_F)t+\theta_0)}, \quad (2)$$

where

$$\tau_p = p\Delta_\tau \quad (3a)$$
$$t_b = b\Delta_b \quad (3b)$$
$$f_F = f_i + F\Delta_f \quad (3c)$$

represent the code phase, navigation data bit delay, and Doppler frequency hypotheses made by the receiver, respectively, and $\Delta_\tau = 0.5[1/R_c]$, $1 \le \Delta_b \le 10$, and $\Delta_f = 1/(2T)$ [Hz] are the search step sizes for the code phase, navigation data bit boundary, and Doppler frequency used in this paper, respectively. The quantity f_i is the lowest possible Doppler frequency of $y(t)$, and $p = 0, 1, \ldots, p_m - 1$, $b = 0, 1, \ldots, b_m - 1$, and $F = 0, 1, \ldots, F_m - 1$ are the indices of the code phase, bit boundary, and Doppler frequency hypotheses, respectively. Therefore,

$$p_m = L_c/\Delta_\tau \quad (4a)$$
$$b_m = 20/\Delta_b. \quad (4b)$$

Let $\mathbf{D}_i$ be the i-th navigation data sequence hypothesis in $\mathbf{S}_D$ that includes all possible navigation data sequences during T such that

$$\begin{aligned}\mathbf{D}_i \in \mathbf{S}_D &= \{\{+1,+1,\ldots,+1\},\{+1,\ldots,+1,-1\},\ldots,\\ &\quad \{+1,-1,\ldots,-1\}\}\\ &= \{D_1, D_2, \ldots, D_{N_s}\}\end{aligned} \quad (5)$$

where $\|\mathbf{D}_i\|_0 = R_b + 1$, $1 \le i \le N_s$, and $N_s = 2^{R_b}$ is the number of all possible sets of navigation data sequences relative to the first data bit within T for $R_bT_b \le T < (R_b+1)T_b$. Considering the code phase, Doppler frequency, navigation data, and bit boundary, the auto-correlation function (ACF) output can be expressed as a four-Dimensional function as

$$R_4[p, F, i, b] = \frac{1}{T}\int_{t_0}^{t_0+T} y(t)x(t)^* dt, \quad (6)$$

where $(\cdot)^*$ denotes the complex conjugate operation. Notice that we use the continuous-time mathematical expression in (6) for algebraic simplicity.

For coherent integration [14] with long correlation interval T, the number of total hypotheses to test to completely define $\mathbf{R}_4$ (6) can be as large as

$$N_{co}^H = p_m F_m b_m N_s. \tag{7}$$

For example, for $T = 0.5$ s, $\Delta_\tau = 0.5T_c$ and $\Delta_b = 5$, it results in $N_{co}^H \simeq 2^{51}$.

III. Component Algorithms for Low Computational Detection

In this section, we introduce the key component algorithms that used to realize the proposed technique described in Section IV. Note that some of the key variables used in this section are described in Table II.

A. Estimating Test Results of Close Doppler Frequency Hypotheses

In this subsection, we derive algebraic expressions to estimate the test result (i.e., ACF output) of a Doppler frequency hypothesis utilizing the test result of a close Doppler frequency hypothesis. This algorithm can be applied to multiple successive ACF outputs over time, making the estimation of the test result of a Doppler frequency hypothesis with a long coherent integration interval T possible with the test results of a close Doppler frequency hypotheses over multiple short coherent intervals.

When $T = T_1$, it can be assumed that $\mathbf{D}_i = D$ (constant) without loss of generality, and, as a result, $\mathbf{R}_4$ (6) collapses to a 2-Dimensional function $\mathbf{R}_2$ whose continuous-time mathematical expression is already available in [8] and is written below

$$\begin{aligned} &R_4[p, F, i, b]|_{T=T_1} \\ &\quad = \frac{AD}{T_1}\int_{t_0}^{t_0+T_1} P(t-\tau_k)P(t-\tau_p)e^{j(2\pi\delta_F t+\phi)}dt + w \\ &\quad = \frac{AD\sin(\pi\delta_F T_1)}{\pi\delta_F T_1} \times \frac{\sin(\pi\delta_F(T_c-|\delta_\tau|))}{\sin(\pi\delta_F T_c)} \\ &\qquad \times e^{j(2\pi\delta_F t_0+\pi\delta_F T_1-\pi\delta_F|\delta_\tau|+\phi)} + w \\ &\quad = R_2[p, F], \end{aligned} \tag{8}$$

where $\delta_F = f_D^k - f_F$, $\delta_\tau = \tau_k - \tau_p$, and

$$\begin{aligned} w &= \frac{1}{T_1}\int_{t_0}^{t_0+T_1}\Bigg[\sum_{v=1, v\neq k}^{K} A^v D^v(t-\tau_v)P^v(t-\tau_v) \\ &\qquad \times e^{j(2\pi(f_I+f_D^v)t+\theta_v)} + v(t)\Bigg]x(t)^* dt \\ &\simeq \frac{1}{T_1}\int_{t_0}^{t_0+T_1} v(t)x(t)^* dt \end{aligned} \tag{9}$$

is a complex Gaussian noise with two-sided power spectral density $N_0/2$.

The goal is to enhance the sensitivity of a GPS receiver by extending T much larger than T_1 such that $T = R_T T_1 \gg T_1$, while employing high sampling rate f_s allowed by the receiver hardware. Let the expression in (8) is over an interval T_1 within a much wider interval $[0, T]$ such that $[lT_1, (l+1)T_1] \subset [0, T]$, where $0 \le l < R_T$, then we can

$$\begin{aligned} &R_4[p, F, i, b]|_{t_0=lT_1, T=T_1} \\ &\quad = AD\frac{\sin(\pi\delta_F T_1)}{\pi\delta_F T_1} \times \frac{\sin(\pi\delta_F(T_c-|\delta_\tau|))}{\sin(\pi\delta_F T_c)} \\ &\qquad \times e^{j((2l+1)\pi\delta_F T_1-\pi\delta_F|\delta_\tau|+\phi)} + w \\ &\quad = R_3[l, p, F]. \end{aligned} \tag{10}$$

When $|\delta_\tau| \ll T_c$, (10) can be further simplified to

$$R_3[l, p, F] \simeq \frac{AD\sin(\pi\delta_F T_1)}{\pi\delta_F T_1} e^{j((2l+1)\pi\delta_F T_1+\phi)} + w. \tag{11}$$

Note that (11) reveals the phase change of R_3 with respect to l and F. From (11), it can be found that, for a fixed l, small frequency index offset f_o, and $|\delta_\tau| \ll T_c$

$$\begin{aligned} &E\left[R_3[l, p, F+f_o]\right] \\ &\quad \simeq \frac{AD\sin\left[\pi(\delta_F - f_o\Delta_f)T_1\right]}{\pi(\delta_F - f_o\Delta_f)T_1} e^{j[(2l+1)\pi(\delta_F - f_o\Delta_f)T_1+\phi]}, \end{aligned} \tag{12}$$

from which we develop a relationship between (11) and (12) as

$$\begin{aligned} &E\left[R_3[l, p, F+f_o]\right]\frac{\sin(\pi\delta_F T_1)}{\pi\delta_F T_1} e^{j(2l+1)\pi f_o\Delta_f T_1} \\ &\qquad \simeq E\left[R_3[l, p, F]\right]\frac{\sin\left[\pi(\delta_F - f_o\Delta_f)T_1\right]}{\pi(\delta_F - f_o\Delta_f)T_1}. \end{aligned} \tag{13}$$

The above expression (13) verifies that the amplitude and phase of the ACF output for a close Doppler frequency hypothesis with an index $F + f_o$ can be estimated by utilizing the ACF output for a Doppler frequency hypothesis with a neighboring or close index F. Note that since the $sinc(\cdot)$ function in (13) is an even function, $E[R_3[l, p, F]]$ can be used to estimate $E[R_3[l, p, F - f_o]]$, too. Inversely, when the correct Doppler frequency hypothesis index is $F + f_o$ and $R_3[l, p, F]$ is obtained, we can estimate $R_3[l, p, F + f_o]$ as

$$\begin{aligned} &E\left[R_3[l, p, F]\right]\frac{\sin\left[\pi(\delta_F - f_o\Delta_f)T_1\right]}{\pi(\delta_F - f_o\Delta_f)T_1} e^{-j(2l+1)\pi f_o\Delta_f T_1} \\ &\qquad \simeq E\left[R_3[l, p, F+f_o]\right]\frac{\sin(\pi\delta_F T_1)}{\pi\delta_F T_1}. \end{aligned} \tag{14}$$

The expressions in (13) and (14) show that the estimated amplitude of the ACF outputs (i.e., $R_3[l, p, F]$ and $R_3[l, p, F + f_o]$, respectively) are slightly smaller than the true value. Fig. 1 shows the magnitude and phase of the estimated ACF output $E[R_3[l, p, F + f_o]]$ using $E[R_3[l, p, F]]$ with respect to f_0 in unit of $1/(2T)$Hz. Note that the amplitude decrease of $E[R_3[l, p, F + f_o]]$ in (14) and in Fig. 1 does not imply the decreased noise power as well. However, from (14), when the frequency offset f_o satisfies

$$|f_o\Delta_f T_1| \ll 1, \tag{15}$$

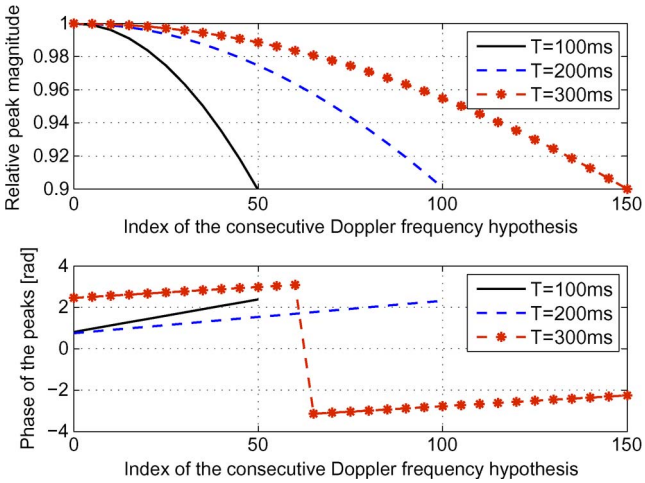

Fig. 1. Peak amplitude degradation in SDFT.

the amplitude decrease of $E[R_3[l, p, F \pm f_o]]$ is negligibly small so that the SNR decrease can be negligible. In a general form, (13) can be written as

$$E\left[R_3[l,p,F]\right] = \alpha(f_o) E\left[R_3[l,p,F+f_o]\right] e^{j(2l+1)\pi f_o \Delta_f T_1}, \quad (16)$$

where

$$\alpha(f_o) \simeq \frac{\sin(\pi f_o \Delta_f T_1)}{\pi f_o \Delta_f T_1}. \quad (17)$$

Since $\Delta_f = 1/(2T)$, the equation (15) is equivalent to $|f_o| \ll 2R_T$, and

$$|f_o| \le \frac{2R_T}{M_f} = f_m, \quad (18)$$

is a useful condition to have $\alpha(f_o) \simeq 1$ for $1 \ll M_f \ll R_T$. Fig. 1 shows that the peak amplitude of ACF output decreases only about 10% (i.e., $\alpha(f_o) = 0.9$) when $f_o = R_T/2$. Therefore, we use the maximum allowed Doppler frequency offset $f_m = R_T/2$ to estimate and the maximum frequency offset factor $M_f = 4$ in this paper.

When the indices of the correct navigation data D_i and bit boundary t_b hypotheses are denoted as i^1 and b^1, respectively, and $1 \ll M_f \ll R_T$,

$$E\left[R_4[p,F,i^1,b^1]\right]$$

$$\simeq \frac{AD}{T}\int_{t_0}^{t_0+T} P(t-\tau)P(t-\tau_p)e^{j(2\pi\delta_F t+\phi)}dt \quad (19a)$$

$$\simeq \sum_{l=0}^{R_T-1} E\left[R_3[l,p,F]\right] \quad (19b)$$

$$= \alpha(f_o)\sum_{l=0}^{R_T-1} E\left[R_3[l,p,F+f_o]\right] e^{j(2l+1)\pi f_o \Delta_f T_1}. \quad (19c)$$

From (13), (14), and (19c), it is found that the result of a coherent integration with a long interval T and a Doppler frequency hypothesis F (or $F+f_o$) can be estimated from the sum of R_T partial coherent integrations over R_T successive integration segments $[lT_1, (l+1)T_1]$ $(l = 0, 1, \ldots, R_T - 1)$ using a close Doppler frequency hypothesis $F + f_o$ (or F).

Note that instead of the conventional FFT-based coherent correlation technique with a long integration interval T that requires

$$M_c = f_s T[\log_2(f_s T) + 1] \quad (20)$$

complex multiplications to test each Doppler frequency hypothesis, where f_s is the sampling frequency, we exploit (19c) and perform R_T FFT-based partial coherent correlations with a short integration interval T_1, which requires only

$$M_{p,F} = f_s T[\log_2(f_s T_1) + 1] \quad (21)$$

complex multiplications for a Doppler frequency hypothesis. The complexity of the component algorithm derived in this subsection is further reduced by half in the realization of SDHT technique in Section IV-B.

B. Proposed Sample Compression for Fast Processing

To increase the detection sensitivity of a GPS receiver, $f_s \gg 2R_c$ and $B \simeq 2R_c$ are useful choices in practice, and we assume $f_s = q_c R_s R_c$, where q_c and R_s are positive integers larger than 1. Since $f_s \gg 2R_c$ and $T \gg T_1$, the computational cost for a long coherent integration scheme can be huge. In this subsection, we propose a sample compression (SC) technique that reduces the number of signal samples to process to reduce the number of complex multiplications in the acquisition process; the proposed SC technique produces $y_{sc}[n]$ from the original signal samples $y[n]$ that is obtained from $y(t)$ sampled at $t = nT_s = n/f_s$ as

$$y_{sc}[n] = \sum_{m=0}^{R_s-1} y[R_s n + m] e^{-j2\pi(f_I+f_F)(R_s n+m)+\theta_0}, \quad (22)$$

where $R_s = f_s/(q_c R_c)$ is the sample compression rate per chip, and q_c represents the number of compressed samples per chip (T_c) after the SC technique. Note that $q_c = f_s/(R_s R_c) \ge 2$ is required for the conventional code phase search to maintain $\Delta_\tau \le T_c/2$. Note also that the proposed SC technique (22) is different from the averaging correlator (AC) technique [3] in that the AC technique uses $q_c = 1$ to minimize the number of samples to process, and the AC technique needs to test R_s sets of data samples for R_s different chip boundary hypotheses.

Utilizing (19c) and (22), the total number of complex multiplications required for a Doppler frequency hypothesis testing can be as small as

$$M_{p,S} = q_c R_c T\left[\log_2(q_c R_c T_1) + 1\right], \quad (23)$$

which is about $R_s \log_2(f_s T)/\log_2(f_s T_1/R_s)$ times smaller than M_c (20). However, the proposed SC technique can loose SNR depending on the size of q_c. With the SC technique, there are $q_c - 1$ compressed samples with amplitude $R_s A^k$ and one compressed sample with amplitude from 0 to $R_s A^k$ depending on the polarity of the next PRN code chip and sampling offset

to the chip boundary. Considering the randomness of the PRN code and the sampling offset, the expected amplitude of the one compressed sample is $3R_sA^k/4$. As a result, the SNR loss due to the SC technique for $q_c \geq 2$ and $R_s \geq 2$ can be expressed as

$$L_{sc} = 20\log_{10}\left(\frac{1}{R_s q_c}\left[R_s(q_c-1)+\frac{3R_s}{4}\right]\right) = 20\log_{10}\left(1-\frac{1}{4q_c}\right), \quad (24)$$

which is about 1.16 dB and less than 0.56 dB for $q_c = 2$ and $q_c \geq 3$, respectively.

IV. Proposed Low Computational Weak GNSS Signal Detection Technique

In this section, we provide the complete description and step-by-step realization of the proposed low computational weak GNSS signal detection technique. In Section IV-A, we propose the sparse Doppler frequency search (SDFS) technique that tests sparsely located (i.e., with large frequency spacing $1/(2T_1)$) Doppler frequency hypotheses so that the ACF outputs are utilized by the SDHT technique. In Section IV-B, we develop an algebraic expression to further reduce the computational cost in exploiting the component technique derived in Section III-A, which constitutes the SDHT technique that completes the tests of all Doppler frequency hypotheses with a much smaller frequency search step size $1/(2T)(\ll 1/(2T_1))$ and a long coherent integration interval T. In Section IV-C, we provide a brief description of the navigation data and bit boundary hypotheses testing scheme. The SC technique introduced in Section III-B can be applied to both SDSF and SDHT techniques. Note that some of the key variables used in this section are described in Table II in Appendix C.

A. Sparse Doppler Frequency Search (SDFS)

For a long coherent integration interval T and the Doppler frequency range $[-5, 5]$ kHz, the conventional GNSS signal acquisition techniques need to test total

$$F_m = 2\times 10^4 T + 1 \quad (25)$$

Doppler frequency hypotheses. However, using (16) and (18) with $T_1 = 1$ ms, we can restrict the number of Doppler frequency hypotheses to be tested with actual correlations to

$$F_{n,1} = 10^4 T/f_m + 1 = 5M_f + 1, \quad (26)$$

which is only 21 Doppler frequencies evenly distributed with $2f_m\Delta_f$Hz spacing. In this paper, we call the actual correlation operations for the 21 sparsely located Doppler frequency hypotheses the sparse Doppler frequency search (SDFS) in comparison to the narrowly spaced $F_m(\gg 21)$ Doppler frequency hypotheses to be tested for $T \gg T_1$. Note that $2f_m\Delta_f$Hz is a sufficient Doppler frequency spacing to apply the SDHT technique, however, the Doppler frequency spacing can be smaller or larger than $2f_m\Delta_f$Hz depending on the SNR loss allowed.

In the following analysis, we exploit the FFT-based technique in [2] as one of the common implementation schemes for GNSS receivers. Let $l = 0$ and $f_c = 0$ represent the first partial correlation with a short interval T_1 and the first sparse Doppler frequency hypothesis in SDFS, respectively. The 1st step of the SDFS is to obtain a pseudo-baseband signal samples of the received signal

$$y[n] = y(nT_s)e^{-j2\pi f_l n T_s}, \quad (27)$$

for $n = 0, 1, \ldots, f_sT - 1$. The 2nd step is to apply the SC technique (22) to $y[n]$ to obtain $y_{sc}[n]$. Note that $y[n]$ has at most 5 kHz Doppler frequency, and that the SC technique integrates the successive samples of $y[n]$ within an interval much narrower than a chip width $T_c(\simeq 1\ \mu$s). Therefore, we can neglect the effect of phase difference between the samples of $y[n]$ and assume there is no distortion to the signal due to the SC technique.

Let q_1 be the number of compressed samples of $\mathbf{y}_{sc}(= \{y_{sc}[n]|n = 0, 1, \ldots, f_sT_1/R_s - 1\})$ within T_1, and let Q_1 be the smallest integer power of 2 that is greater than or equal to $2q_1$ (i.e., $Q_1 \geq 2q_1$) required for FFT operation. The 3rd step is to perform Q_1-point FFT of $\mathbf{y}^z_{sc}$, that is $\mathbf{y}_{sc}$ padded with $Q_1 - q_1$ zeros as

$$y^z_{sc}[n] = \begin{cases} y_{sc}[n], & 0 \leq n < q_1 \\ 0, & q_1 \leq n < Q_1, \end{cases} \quad (28)$$

to develop $\mathbf{Y}^F_{sc}$. The 4th step is to perform the FFT-based correlation $\mathbf{Y}^F_{sc}\cdot(\mathbf{X}^F)^*$, where $(\cdot)$ represents the inner product operation, where $(\mathbf{X}^F)^*$ is the complex conjugate of the Q_1-point FFT output of $x[n]$ obtained by sampling

$$x(t) = P(t-\tau_p)e^{-j2\pi(f_i+\Delta_f f_c)nT_s} \quad (29)$$

at a sampling frequency q_cR_c, and f_c is an index of

$$\mathbf{f}_c = \{0, 2f_m, \ldots, 10M_f f_m\} \quad (30)$$

representing the set of sparse Doppler frequencies spaced at $2f_m\Delta_f$Hz apart. And the 5th step uses the first q_1 samples of $\mathbf{R}_{yx}$, the Q_1-point IFFT output of $\mathbf{Y}^F_{sc}\cdot(\mathbf{X}^F)^*$, to obtain an ACF output $\mathbf{R}_3$ as

$$\mathbf{R}_3[l, q, 2f_m f_c] = \begin{cases} \mathbf{R}_{yx}(q), & 0 \leq q < q_1 \\ 0, & q_1 \leq q < Q_1, \end{cases} \quad (31)$$

where $l = 0$ and $f_c = 0$. The above five steps are repeated with new signal samples for successive integration intervals $[lT_1, (l+1)T_1]$ for all $l \in \mathbf{l} = \{0, 1, \ldots, R_T - 1\}$, and, as a result, we build $\mathbf{R}_3[\mathbf{l}, \mathbf{q}_1, 0]$, where $\mathbf{q}_1 = \{0, 1, \ldots, q_1 - 1\}$. Furthermore, by repeating the above procedure with $f_c = 1$, the receiver can obtain $\mathbf{R}_3[\mathbf{l}, \mathbf{q}_1, 2f_m]$, ACF outputs at the next sparse Doppler frequency hypothesis, and, likewise, the receiver can obtain $\mathbf{R}_3[\mathbf{l}, \mathbf{q}_1, \mathbf{f}_c]$ and complete SDFS. Each ACF output of the SDFS, the ACF output for each f_c of matrix $\mathbf{R}_3[\mathbf{l}, \mathbf{q}_1, \mathbf{f}_c]$, is tested for the navigation data and bit boundary hypotheses, which is briefly described in Section IV-C.

Note that the SR technique [4] can be used to construct $\mathbf{Y}_{sc}^{F}$; $\mathbf{Y}_{sc}^{F}$ is computed for R_T successive short coherent intervals, and, for each of $F_{n,1}$ sparse Doppler frequency hypotheses, SDFS performs circular shift of $\mathbf{Y}_{sc}^{F}$ to change Doppler frequency hypothesis, $R_T Q_1$ frequency-domain multiplications, R_T times Q_1-point IFFT operation, and R_T times phase compensation to the q_1-elements of the IFFT outputs. Therefore, exploiting the SR technique and assuming $(\mathbf{X}^F)^*$ is pre-computed and stored in a memory of the receiver [2], the number of complex multiplications for SDFS is $R_T Q_1 \log_2 Q_1 + (5M_f + 1)R_T[Q_1 \log_2 Q_1 + Q_1 + q_1]$.

B. Synthesized Doppler Frequency Hypothesis Testing (SDHT)

When no signal detection is declared at the end of the SDFS, we estimate another set of new ACF outputs $\mathbf{R}_3[\mathbf{l}, \mathbf{q}_1, \mathbf{f}_c^{(1)}]$ for the $5M_f$ intermediate Doppler frequency hypotheses in-between every two neighboring Doppler frequency hypotheses tested in SDFS, where

$$\mathbf{f}_c^{(1)} = \{f_m, 3f_m, \ldots, (10M_f - 1)f_m\}. \tag{32}$$

The new ACF output matrix $\mathbf{R}_3[\mathbf{l}, \mathbf{q}_1, \mathbf{f}_c^{(1)}(m_f)]$ for a intermediate Doppler frequency $\mathbf{f}_c^{(1)}(m_f)$ (where m_f is an index in $0 \le m_f < 5M_f$) is easily estimated with the algebraic sum of $\mathbf{R}_3[\mathbf{l}, \mathbf{q}_1, \mathbf{f}_c(m_f)]$ and $\mathbf{R}_3[\mathbf{l}, \mathbf{q}_1, \mathbf{f}_c(m_f+1)]$; the sum of two ACF outputs, for the same $l \in \mathbf{l}$ and $q \in \mathbf{q}_1$ and any neighboring sparse Doppler frequency hypotheses $\mathbf{f}_c(m_f)$ and $\mathbf{f}_c(m_f+1)$, becomes

$$\begin{aligned}
&\mathbf{R}_3[l, q, 2f_m m_f] + \mathbf{R}_3[l, q, 2f_m(m_f+1)] \\
&\quad = E\left[\mathbf{R}_3[l, q, 2f_m m_f]\right] + E\left[\mathbf{R}_3[l, q, 2f_m(m_f+1)]\right] \\
&\qquad + \int_{lT_1}^{(l+1)T_1} \frac{2v(t)P(t-\tau_q)}{T_1} e^{j2\pi[f_i + f_m(2m_f+1)]\Delta_f t} \\
&\qquad \times \cos(2\pi f_m \Delta_f t) dt \\
&\quad = 2\alpha(f_m) \cos\left(\frac{(2l+1)\pi f_m}{2R_T}\right) E\left[\mathbf{R}_3[l, q, f_m(2m_f+1)]\right] \\
&\qquad + \int_{l_o}^{l_o+T_1} \frac{2v'(t)}{T_1} \cos(2\pi f_m \Delta_f t) dt \\
&\quad = 2\alpha(f_m) \cos(\frac{(2l+1)\pi f_m}{2R_T}) E\left[\mathbf{R}_3[l, q, f_m(2m_f+1)]\right] + w' \qquad \text{(33a)} \\
&\quad = \mathbf{R}_3^{(1)}[l, q, f_m(2m_f+1)], \qquad \text{(33b)}
\end{aligned}$$

where

$$v'(t) = v(t)P(t-\tau_q)e^{-j2\pi[f_i + f_m(2m_f+1)]\Delta_f t} \tag{34a}$$

$$w' = \int_{lT_1}^{(l+1)T_1} \frac{2v'(t)}{T_1} \cos(2\pi f_m \Delta_f t) dt, \tag{34b}$$

and the notation $\mathbf{R}_3^{(1)}$ in (33b) represents the weighted ACF output matrix estimated using the proposed SDHT technique for Doppler frequency hypotheses in $\mathbf{f}_c^{(1)}$. Note that $v'(t)$ (34a) has the same PSD to $v(t)$ in (1), and that w' (34b) has $\sqrt{2}$ times the PSD of $v'(t)$. Note also that the cosine term in (33a) never becomes zero, since R_T is an integer power of 2 and $f_m \ll R_T$. Computing (33b) for all $l(\in \mathbf{l} = \{0, 1, \ldots, R_T - 1\})$, $q(\in \mathbf{q}_1 = \{0, 1, \ldots, q_1 - 1\})$, and $m_f(\in \{0, 1, \ldots, |\mathbf{f}_c^{(1)}\|_0 - 1\})$ produces $\mathbf{R}_3^{(1)}[\mathbf{l}, \mathbf{q}_1, \mathbf{f}_c^{(1)}]$.

The weighted ACF matrix $\mathbf{R}_3^{(1)}$ for each Doppler frequency in $\mathbf{f}_c^{(1)}$ is then de-weighted to estimate the normalized ACF matrix $\mathbf{R}_3$ and tested for navigation data and bit boundary hypotheses described in Section IV-C. The de-weighting of $\mathbf{R}_3^{(1)}$ is to multiply $0.5[\cos[(2l+1)\pi f_m/(2R_T)]]^{-1}$ to the l-th row of $\mathbf{R}_3^{(1)}$ for all $l \in \mathbf{l}$ such that

$$\begin{aligned}
&\frac{0.5}{\cos\left(\frac{(2l+1)\pi f_m}{2R_T}\right)} \mathbf{R}_3^{(1)}[l, \mathbf{q}_1, f_m(2m_f+1)] \\
&\quad = \alpha(f_m) E\left[\mathbf{R}_3[l, \mathbf{q}_1, f_m(2m_f+1)]\right] + \frac{0.5w'}{\cos\left(\frac{(2l+1)\pi f_m}{2R_T}\right)} \\
&\quad = \alpha(f_m) E\left[\mathbf{R}_3[l, \mathbf{q}_1, f_m(2m_f+1)]\right] + w''. \qquad \text{(35)}
\end{aligned}$$

Note that $E[\mathbf{R}_3[l, \mathbf{q}_1, f_m(2m_f+1)]]$ is estimated from a simple sum in (33a) and a real value multiplication with $\alpha(f_m)$, which further saves computational cost from the component technique derived in Section III-A. Note also that for $f_m = R_T/2$

$$\left|\cos\left(\frac{(2l+1)\pi f_m}{2R_T}\right)\right|^{-1} = \sqrt{2}, \tag{36}$$

so that w'' has the same PSD to w in (9), and since $\alpha(f_m) \simeq 0.9$ when $f_m = R_T/2$ as shown in Fig. 1, a slight SNR loss (about 1 dB) is expected in the ACF output estimated by the SDHT technique. In a matrix form, (35) can be equivalently expressed as

$$\begin{aligned}
&\mathbf{C}^{(1)} \mathbf{R}_3^{(1)}[\mathbf{l}, \mathbf{q}_1, f_m(2m_f+1)] \\
&\qquad = \alpha(f_m) E\left[\mathbf{R}_3[\mathbf{l}, \mathbf{q}_1, f_m(2m_f+1)]\right] + w'' \qquad \text{(37)}
\end{aligned}$$

where

$$C^{(1)}(l, q) = \frac{1}{2}\left[\cos\frac{(2l+1)\pi f_m}{2R_T}\right]^{-1} \delta[l-q], \tag{38}$$

and $\delta[l-q]$ is the Dirac delta function [16]. As a result, SDFS in Section IV-A and $\mathbf{R}_3^{(1)}$ complete Doppler frequency hypothesis tests for a finer Doppler frequency search resolution $f_m \Delta_f$.

Similar procedure can be used to estimate ACF output matrices with much finer Doppler frequency hypotheses. Using $\mathbf{R}_3[\mathbf{l}, \mathbf{q}_1, \mathbf{f}_c]$ (31) and $\mathbf{R}_3[\mathbf{l}, \mathbf{q}_1, \mathbf{f}_c^{(1)}]$ (37), we can estimate $\mathbf{R}_3^{(2)}$ for $10M_f$ intermediate Doppler frequency hypotheses with indices

$$\mathbf{f}_c^{(2)} = \left\{\frac{1}{2}f_m, \frac{5}{2}f_m, \ldots, \frac{20M_f - 1}{2}f_m\right\} \tag{39}$$

at the middle of every two neighboring Doppler frequency hypotheses in $\mathbf{f}_c \cup \mathbf{f}_c^{(1)}$ as

$$\begin{aligned}
&\mathbf{R}_3[l, \mathbf{q}_1, 2f_m m_f] + \alpha(f_m) E\left[\mathbf{R}_3[l, \mathbf{q}_1, f_m(2m_f+1)]\right] + w'' \\
&\quad \simeq 2\alpha\left(\frac{f_m}{2}\right) \alpha(f_m) E\left[\mathbf{R}_3\left[l, \mathbf{q}_1, f_m\left(2m_f + \frac{1}{2}\right)\right]\right] \\
&\qquad \times \cos\left(\frac{(2l+1)\pi f_m}{4R_T}\right) + w_1' \qquad \text{(40a)} \\
&\quad \simeq 2\alpha(f_m) E\left[\mathbf{R}_3\left[l, \mathbf{q}_1, f_m\left(2m_f + \frac{1}{2}\right)\right]\right] \cos\left(\frac{(2l+1)\pi f_m}{4R_T}\right) \\
&\qquad + w_1' \qquad \text{(40b)} \\
&\quad \simeq \mathbf{R}_3^{(2)}\left[l, \mathbf{q}_1, f_m\left(2m_f + \frac{1}{2}\right)\right], \qquad \text{(40c)}
\end{aligned}$$

and

$$\alpha(f_m)E\left[\mathbf{R}_3[l,\mathbf{q}_1,f_m(2m_f+1)]\right]+\mathbf{R}_3\left[l,\mathbf{q}_1,2f_m(m_f+1)\right] + w'' \simeq \mathbf{R}_3^{(2)}\left[l,\mathbf{q}_1,f_m\left(2m_f+\frac{3}{2}\right)\right], \quad (41)$$

for $m_f = 0, 1, \ldots, 5M_f - 1$, where w_1' is a complex Gaussian noise with the same PSD to w' in (33a), and, based on Fig. 1, $\alpha(f_m/2) \simeq 1$ is assumed. By de-weighting $\mathbf{R}_3^{(2)}$ in (40c) and (41), we now complete all the Doppler frequency hypothesis tests for a Doppler frequency search step size $f_m\Delta_f/2$.

In a general form,

$$\mathbf{R}_3^{(h)}\left[\mathbf{l},\mathbf{q}_1,f_m\left(2m_f+\frac{2g-1}{2^{h-1}}\right)\right] = \sum_{i=0}^{1}\mathbf{R}_3\left[\mathbf{l},\mathbf{q}_1,f_m\left(2m_f+\frac{2g-2i}{2^{h-1}}\right)\right], \quad (42a)$$

and

$$\mathbf{R}_3\left[\mathbf{l},\mathbf{q}_1,f_m\left(2m_f+\frac{2g-1}{2^{h-1}}\right)\right] = \mathbf{C}^{(h)}\mathbf{R}_3^{(h)}\left[\mathbf{l},\mathbf{q}_1,f_m\left(2m_f+\frac{2g-1}{2^{h-1}}\right)\right], \quad (42b)$$

where $h = 1, 2, \ldots, \lceil 1+\log_2 f_m\rceil$, $g = 1, 2, \ldots, 2^{h-1}$, and

$$C^{(1)}(l,q) = \frac{1}{2}\left[\cos\frac{(2l+1)\pi f_m}{2^h R_T}\right]^{-1}\delta[l-q]. \quad (43)$$

The process in (42a) and (42b) realizes the SDHT technique. Each of $2^{h-1}\times 5M_f$ ACF matrices $\mathbf{R}_3$ computed from (42a) and (42b) is tested for the navigation data and bit boundary hypotheses introduced in Section IV-C. Similarly, when no signal detection is declared after all R_3 (42b) are tested, we increase h by one and repeat the SDHT, which can continue until $2^{1-h}f_m\Delta_f \le \Delta_f$, or, equivalently, until $h = 1+\log_2 f_m$ for f_m an integer power of 2.

Fig. 2 demonstrates the performance of the SDHT in terms of the post-correlation SNR of $\mathbf{R}_3$ obtained from Monte Carlo simulations. It shows the plots of $\sum_{l=0}^{R_T}\mathbf{C}^{(h)}\mathbf{R}_3^{(h)}$, where the horizontal axis is the relative code phase from the true code phase, and the effect of navigation data and sample compression is not considered to see the pure effect of SDHT only on SNR. The simulation is performed for a GPS L1 C/A code signal with $C/N_0 = 40$ dB-Hz and a receiver using $B = 2.046$ MHz, $f_s = 12R_c$, and $R_T = 16$. Note that the expected post-correlation SNR is supposed to be 20 dB when Doppler frequency hypothesis test is actually performed using the conventional correlation technique. However, when the SDHT is used with $f_m = R_T/2 = 8$, it shows that the post-correlation SNR has about 1 dB loss, since $\alpha(f_m) \simeq 0.9$ as expected. And when $f_m = 12 > R_T/2$, SNR loss larger than 1 dB is expected as $\alpha(f_m) < 0.9$.

Since there are maximum

$$F_{n,2} = F_m - F_{n,1} = F_m - 5M_f - 1 = 5M_f(2f_m - 1) \quad (44)$$

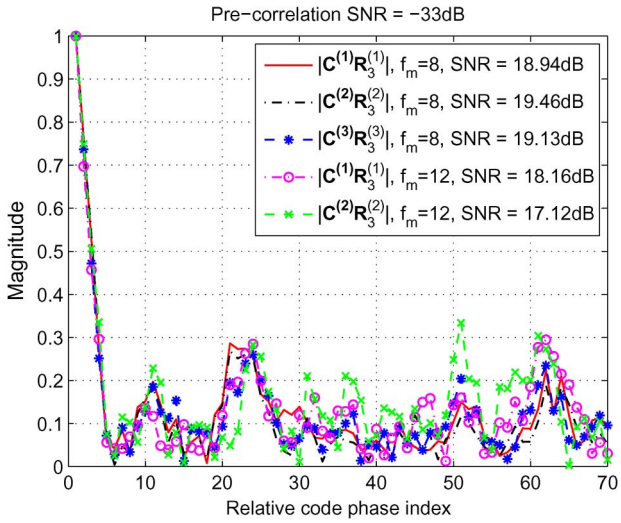

Fig. 2. Probability of detection w.r.t. the SNR of y_0.

Doppler frequency hypotheses to test with the SDHT technique, both the maximum number of real multiplications and that of complex additions are equal to

$$N_M = q_1 R_T F_{n,2} \quad (45)$$

to complete the estimation of $\mathbf{R}_3$ for all R_T partial coherent integrations with an interval T_1, q_1 code phases, and F_m Doppler frequencies. Note that, to apply SDHT, $\mathbf{R}_3$ in (42a) and (42b) should be obtained with the same received signal samples so that $\mathbf{R}_3$ contains the same navigation data.

C. Navigation Data and Bit Boundary Hypothesis Testing

In this subsection, we explain a simple algorithm for the navigation data and bit boundary hypothesis testing with a given ACF output. For a given Doppler frequency hypothesis with an index F, $\mathbf{R}_3$ obtained in the Section IV-A and Section IV-B can be expressed by two-dimensional matrix $\mathbf{R}_2[\mathbf{l},\mathbf{q}_1] = \mathbf{R}_3[\mathbf{l},\mathbf{q}_1,F]$ of size $[R_T\times q_1]$. And, for algebraic simplicity, we assume that $R_T T_1 = R_b T_b$ so that R_T is a multiple of 20, since $T_1 = 1$ ms and $T_b = 1$ ms.

Since $\mathbf{R}_2$ is built with R_T successive ACF outputs, there are R_b or R_b+1 navigation data bits that contribute to $\mathbf{R}_2$. Let

$$\mathbf{b}_i^u = \left[b_0^u, b_1^{20}, \ldots, b_{R_b-1}^{20}, b_{R_b}^{20-u}\right] \quad (46)$$

define the sample vector of the navigation data signal $D^k(t)$ obtained at a sampling frequency $1/T_1$ [Hz] for the overall coherent integration interval T, i.e., $\mathbf{b}_i^u$ is of size $[1\times R_T]$, where i represents the index of $\mathbf{S}_D$ such that

$$\mathbf{S}_D[i] = \mathbf{D}_i = [b_0, b_1, \ldots, b_{R_b-1}, b_{R_b}], \quad (47)$$

and b_g^u represents u times occurrence of the g-th navigation bit b_g ($\in\{1,-1\}$). Since there are 2^{R_b} different sets of $\mathbf{b}_i^u$ assuming $b_0 = 1$, and considering the bit boundary search step size Δ_b,

there are $2^{R_b}T_b/(T_1\Delta_b)$ hypotheses for the navigation data and bit boundary combination, and u in (46) is assumed in unit of Δ_b. Let $\mathbf{B}$ be a matrix whose columns are the successive samples of navigation data $D^k(t)$ sampled at $1/T_1$ [Hz], then the size of $\mathbf{B}$ is $[2^{R_b}T_b/(T_1\Delta_b) \times R_T]$. Taking the product of $\mathbf{B}$ and $\mathbf{R}_2$ and absolute operation yields a size $[2^{R_b}T_b/(T_1\Delta_b) \times q_1]$ matrix

$$\mathbf{Y}_F = |\mathbf{B}\mathbf{R}_2|, \tag{48}$$

which contains coherent ACF outputs for all possible combinations of code phase, navigation data, and bit boundary hypotheses for a given Doppler frequency hypothesis (with an index F) and the overall integration interval T.

Note that the matrix multiplication in (48) can be effectively performed using only $2^{R_b}q_1(R_T-1)T_b/(T_1\Delta_b)$ times of complex additions or complex subtractions, since the elements of $\mathbf{B}$ are just $+1$'s and -1's. In addition, finding the maximum of $\mathbf{Y}_F$ does not require to take absolute operation in (48) for all elements; since we can estimate the noise variance V_0 (52b), elements of $\mathbf{Y}_F$ whose real and imaginary magnitudes are smaller than $\sqrt{V_0}$ may be eliminated in the absolute operation. Note also that, when the Doppler frequency hypothesis is correct, there can be only one ACF output in $\mathbf{Y}_F$ that contains the coherent sum of signal energy in $r(t)$ for T seconds and is expected to have the maximum ACF peak magnitude. Letting $\mathbf{Y}_{\max}$ be a size $[1 \times F_m]$ vector whose F-th element is the maximum element of $\mathbf{Y}_F$ (i.e., $\mathbf{Y}_{\max}(F) = \max \mathbf{Y}_F$), $\mathbf{Y}_{\max}$ can be used to find the index of the correct Doppler frequency hypothesis of the incoming signal as

$$\hat{F} = \arg\max_F \mathbf{Y}_{\max}, \tag{49}$$

and, then, the maximum element of $\mathbf{Y}_{\hat{F}}$ is used to estimate the indices of the correct code phase, navigation data, and bit boundary hypotheses of the incoming signal as

$$[\hat{p}, \hat{i}, \hat{b}] = \arg\max_{p,i,b} \mathbf{Y}_{\hat{F}}. \tag{50}$$

Note that the maximum element of $\mathbf{Y}_{\hat{F}}$ indicates the correct code phase within Δ_τ, but the navigation data and the bit boundary found with $\mathbf{Y}_{\hat{F}}$ may not be always correct. For example, if all the navigation data bits are $+1$'s, the data bit boundary is obscure and $\mathbf{Y}_{\hat{F}}$ can have $T_b/(T_1\Delta_b)$ similar amplitude peaks. In addition, when u is small (for example, $u < 5$) in (46), correct detection of the first data bit may be difficult and a false bit detection can occur, of which effect on the post-correlation SNR, however, may be negligible.

V. Performance Analysis

In this section, the performance of the proposed technique based on SDFS and SDHT is analyzed in terms of mean acquisition time (MAT) [14] and mean acquisition computation (MAC). We exploit the FFT-based (parallel acquisition) technique in additive white Gaussian noise (AWGN) channels. The SNR of the detection variable $Z = \max \mathbf{Y}^2_{\hat{F}}$ is defined as [9]

$$\text{coherent SNR of } Z\,[\text{dB}] = 10\log_{10}\frac{E[Z]}{V_0}, \tag{51}$$

where

$$E[Z] = (AT_1R_T)^2 \tag{52a}$$

$$V_0 = N_0T_1R_T. \tag{52b}$$

The detection variable Z is then compared to a detection threshold γ to confirm the detection. Therefore, the detection variable and the decision scheme of the proposed technique are identical to those of the conventional parallel coherent correlation technique using FFT, i.e., the FFT-based technique [9]. As a result, the receiver operating characteristic (ROC) of the proposed technique has a very similar performance to the conventional technique except that there is about 1 dB SNR loss in the detection variable due to the SC technique.

Since the proposed technique employs an FFT-based parallel search over the entire code phase space, there are two different types of false alarms possible [17]; a false alarm with probability P_F under the correct Doppler frequency hypothesis H_1^{DF} and another false alarm with probability P_f under an incorrect Doppler frequency hypothesis H_0^{DF}. The P_F, P_f, detection probability P_D, and miss probability P_M of the proposed technique are readily available from [17] and written in Appendix A. Mathematical expression for the MAT of the proposed technique employed in FFT-based technique can be easily found by exploiting those expressions in the conventional parallel search technique [14].

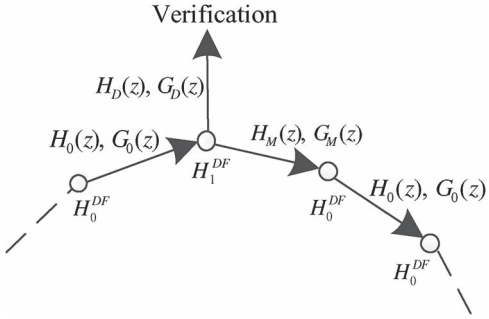

Fig. 3. Circular search state diagram of FFT-based technique.

Fig. 3 illustrates the circular search state diagram of the proposed technique, where an arrow represents an FFT-based parallel code phase hypothesis testing for a Doppler frequency hypothesis H^{DF} represented by a node. The overall transfer function $H(T)$ and branch transfer functions shown in Fig. 3 are written in Appendix B. Note that, in (61), (62a), (62b), and (62c), it is assumed that it takes T seconds to test $\mathbf{R}_3$ for each Doppler frequency hypothesis in (31) and (42b) (i.e., for each $h \in \{0, 1, \ldots, \log_2 f_m\}$). However, the proposed technique may not require T seconds for each of F_m Doppler frequency hypotheses; depending on the computational speed and capacity of the receiver, the proposed technique may require only T seconds to test $2f_m$ Doppler frequency hypotheses. Assuming enough computational speed and capacity of the receiver, the proposed technique using SDFS and SDHT may spend only

TABLE I
COMPARISON OF TOTAL NUMBER OF COMPLEX MULTIPLICATIONS N_{2D}

	Input Sample Processing	Search	Verification
Proposed Technique	$R_T Q_1 \log_2 Q_1$	$(5M_f+1)R_T(Q_1\log_2 Q_1+Q_1+q_1)$ $+5M_f(f_m-0.5)q_1R_T$	$2p_v\, q_1 R_T$
AC Technique [Coherent]	$q_c R_s \times 2L_c^{'} R_T \log_2(2L_c^{'}R_T)$ $\simeq R_s R_T Q_1 \log_2(2L_c R_T)$	$F_m q_c R_s \times 2L_c^{'} R_T\left(\log_2[2L_c^{'}R_T]+1\right)$ $\simeq F_m R_s R_T Q_1\left(\log_2[2L_c R_T]+1\right)$	$2p_v L_c R_T$
AC Technique [Non-Coherent]	$N_{nc} R_s R_{T_{co}} Q_1 \log_2(2L_c R_{T_{co}})$	$N_{nc}\left(20R_{T_{co}}+1\right)R_s R_{T_{co}} Q_1$ $\times\left(\log_2[2L_c R_{T_{co}}]+1\right)$	$2N_{nc}p_v L_c R_{T_{co}}$
BAP Technique for Weak Signals [Coherent]	$q_1 R_s R_T^2$	$21R_T R_s Q_1[2\log_2(R_s Q_1)+1]$	$2p_v L_c R_T$
BAP Technique for Strong Signals [Coherent]	$q_1 R_s R_T^2$	$R_T R_s Q_1[3\log_2(R_s Q_1)+2]$	$2p_v L_c R_T$
SR Technique [Coherent]	$q_c R_s L_c R_T\left(\log_2[q_c R_s L_c]+\log_2[R_T]+1\right)$ $\simeq q_1 R_s R_T\left(\log_2[q_1 R_s]+\log_2[R_T]+1\right)$	$41\times q_c R_s L_c R_T\left(\log_2[q_c R_s L_c]+1\right)$ $\simeq 41 q_1 R_s R_T\left(\log_2[q_1 R_s]+1\right)$	$2p_v L_c R_T$
SR Technique [Non-Coherent]	$N_{nc} q_1 R_s R_{T_{co}}\left(\log_2[q_1 R_s]+\log_2[R_{T_{co}}]+1\right)$	$41 N_{nc} q_1 R_s R_{T_{co}}\left(\log_2[q_1 R_s]+1\right)$	$2N_{nc}p_v L_c R_{T_{co}}$

$T/(2f_m)$ seconds, in average, to test each Doppler frequency hypothesis. Then the MAT of the proposed technique is found in unit of T exploiting [14] and [15]

$$\mu_T = \frac{1}{2f_m}\left.\frac{dH(T)}{dT}\right|_{T=1} = \frac{1}{2f_m}\left[p_v + \frac{1+p_v P_f}{P_D} + (F_m-1)\left(\frac{1}{P_D}-\frac{1}{2}\right)(1+p_v P_F)\right], \tag{53}$$

where p_v is the number of tests in the verification process. Note that the μ_T in (53) shows the MAT can be $2f_m$ times smaller than the conventional FFT-based (parallel acquisition) technique.

Mean acquisition computation (MAC) in [8] and [15] shows the mean computational cost for the GNSS signal acquisition, therefore, the MAC is an important measure to show the advantage of the proposed technique. The overall transfer function for the computational complexity can be found as [15]

$$G(C) = \frac{G_D(C)\left[1-G_0^{F_m}(C)\right]}{F_m[1-G_0(C)]\left[1-G_M(C)G_0^{(F_m-1)}(C)\right]}. \tag{54}$$

where C denotes the unit computational complexity for a complex multiplication, and the correct hypothesis detection, correct hypothesis missed, and incorrect hypothesis branch transfer functions are found as

$$G_D(C) = P_D C^{N_{c,1}+N_{c,p}} \tag{55a}$$
$$G_M(C) = P_M C^{N_{c,1}} + P_f C^{N_{c,1}+N_{c,p}} \tag{55b}$$
$$G_0(C) = (1-P_F)C^{N_{c,1}} + P_F C^{N_{c,1}+N_{c,p}}, \tag{55c}$$

respectively, where $N_{c,1}$ and $N_{c,p}$ are the average number of complex multiplications for a Doppler frequency hypothesis and that for a verification such that

$$N_{c,1} = \frac{F_{n,1}}{F_m}R_T(Q_1\log_2 Q_1 + Q_1 + q_1) + \frac{F_m - F_{n,1}}{F_m}\frac{R_T q_1}{2} = \frac{R_T}{5M_f\cdot 2f_m+1}\left[(5M_f+1)(Q_1\log_2 Q_1 + Q_1 + q_1) + 5M_f q_1\left(f_m-\frac{1}{2}\right)\right] \tag{56a}$$
$$N_{c,p} = 2p_v\, q_1 R_T, \tag{56b}$$

where the verification process is assumed to perform time-domain correlations between $\mathbf{y}_{sc}^{z}$ (28) and $\mathbf{x}$ (29) for p_v times. The circular search state diagram in Fig. 3 also shows the branch transfer functions (55a), (55b), and (55c), and the MAC of the proposed technique in unit of C can be found as [15]

$$\mu_C = \left.\frac{dG(C)}{dT}\right|_{C=1} = N_{c,p}\left(1+\frac{P_f}{P_D}\right) + \frac{N_{c,1}}{P_D} + (F_m-1) \times (N_{c,1}+N_{c,p}P_F)\left(\frac{1}{P_D}-\frac{1}{2}\right), \tag{57}$$

after some algebraic manipulations. When the C/N_0 is high enough, $P_f \to 0$, $P_F \to 0$ and $P_D \to 1$ so that (57) becomes

$$\mu_C|_{SNR\uparrow} = 2p_v\, q_1 R_T + \frac{R_T}{2}\left[5M_f q_1\left(f_m-\frac{1}{2}\right) + (5M_f+1)(Q_1\log_2 Q_1 + Q_1 + q_1)\right], \tag{58}$$

where the first term is for the verification process and the second term is the average computational cost for the search process.

VI. COMPLEXITY COMPARISON AND NUMERICAL SIMULATIONS

Let N_{2D} be the total number of complex multiplications required to test all the hypotheses in the 2-Dimensional (code phase and Doppler frequency) search space. In Table I, N_{2D}'s of the proposed, AC, and SR techniques are summarized for two cases: long coherent integration with interval $T = R_T T_1$ for data free signals and non-coherent integration for data modulated signals, where R_T is an integer power of 2, $T_1 =$ 1 ms, and N_{nc} is the number of non-coherent accumulation of short coherent integrations with interval $T_{co} = R_{T_{co}} T_1$. In addition, Table I includes N_{2D}'s of the BAP technique and the fast BAP technique for weak and strong GNSS signal detection, respectively. In Table I, the verification processes of the three techniques employ p_v time-domain correlations [18].

A. Computational Cost

In the proposed technique, FFT of Q_1 compressed and zero padded received signal samples (i.e., $\mathbf{y}^z_{sc}$) is performed R_T times, 2 times the second term of (58) are required to search the whole 2D hypotheses space using SDFS and SDHT, and the computation size for the verification process is the same to the first term of (58). For coherent integration, since there are $q_c R_s$ samples per chip and $L_c R_T$ chips in T, the AC technique [3] performs $2L'_c R_T$-point FFT of the zero padded received signal samples for $q_c R_s$ times, the $2L'_c R_T$-point FFT output is multiplied to the (frequency domain) receiver replica signal for $F_m q_c R_s$ times, and $2L'_c R_T$-point IFFT is performed for $F_m q_c R_s$ times, where F_m is the total number of Doppler frequency hypotheses to test (25). Note that padding $2R_T(L'_c - L_c)$ zeros to the received signal samples is necessary for the FFT-based correlation [19]. In the verification process, p_v times of time-domain correlations are performed with sample length $2L_c R_T$ (i.e., 2 samples per chip), where the received signal samples are multiplied by carrier signal samples and code replica signal samples.

In the following, $(\rightarrow M_c)$ represents that there are M_c complex multiplications required to perform the operation described on the left.

The BAP and the fast BAP techniques [5] are for the long coherent integration of weak and strong GNSS signals, respectively. While the fast BAP technique suffers from severe (more than 10 dB) SNR loss due to the squaring of signal samples when SNR is low, the BAP technique does not have SNR loss. The BAP technique generates R_T sets of incoming signal samples multiplied by Doppler frequencies within $[0, \frac{1}{2T_1}]$ spaced at $\frac{1}{2T_1 R_T}$Hz $(\rightarrow R_T \times q_c R_s L_c R_T)$. For each set of samples, the BAP technique averages over blocks and generates zero padded block averaged data of size $R_s Q_1$, performs FFT-based technique on the zero padded block averaged data for all 21 coarse Doppler frequencies spaced at 0.5 kHz within $[-5, 5]$kHz $(\rightarrow 21R_T \times R_s Q_1[2\log_2(R_s Q_1) + 1])$. Note that the frequency shifts for 21 Doppler frequencies are not counted, since it can be done in the frequency domain by circular shifting of the FFT'd samples [4]. In the fast BAP technique, the block averaged data is squared and FFT'd to find the Doppler frequency $(\rightarrow q_c R_s L_c + R_s Q_1 \log_2[R_s Q_1])$, and, then, the estimated Doppler frequency is compensated and additional FFT-based technique is applied to find the code phase $(\rightarrow q_c R_s L_c + R_s Q_1[2\log_2(R_s Q_1) + 1])$, which is performed for each of R_T sets of sample data.

In the SR technique [4] for a long coherent integration, the received signal samples are re-arranged to form a $[q_c R_s L_c \times R_T]$ matrix $\mathbf{U}$, where $q_c R_s L_c$ is the number of total samples per a period of the PRN code, and the input processing sequence is as follows; first, FFTs are applied to the rows of $\mathbf{U}$ and yield $\mathbf{U}^{F,L}$ $(\rightarrow q_c R_s L_c \times R_T \log_2 R_T)$, second, element-wise Doppler compensation is performed by computing $\mathbf{C} \odot \mathbf{U}^{F,L}$ to produce $\mathbf{U}^{C,F}$, where $\mathbf{C}$ is the Doppler compensation matrix and $(\odot)$ is an element-by-element multiplication between two matrices $(\rightarrow q_c R_s L_c R_T)$, and, third, FFTs are applied to the columns of $\mathbf{U}^{C,F}$ and generate $\mathbf{U}^F$ $(\rightarrow R_T \times q_c R_s L_c \log_2[q_c R_s L_c])$. In the search process of the SR technique, the receiver computes FFT of the receiver replica signal to obtain $\mathbf{V}_1^F$ of size $[1 \times q_c R_s L_c]$, performs an element-by-element multiplication with the each columns of $\mathbf{U}^F$ (i.e., $(\mathbf{V}_1^{F*}) \circ \mathbf{U}^F$, where $A_v(\circ)A_M$ represents element-by-element multiplication of vector A_v with the each columns of A_M, $\rightarrow q_c R_s L_c R_T$), and computes column-wise IFFT of $(\mathbf{V}_1^{F*}) \circ \mathbf{U}^F$ $(\rightarrow R_T \times q_c R_s L_c \log_2[q_c R_s L_c])$, which produces R_T ACF function outputs for Doppler frequency hypotheses separated at $1/T$ around a Doppler frequency. This procedure is repeated for 21 circularly shifted vector of $\mathbf{V}_1^F$ to test all 21 coarse Doppler frequencies spaced at 1 kHz from -5 kHz to 5 kHz. The above search process needs to be performed with $\mathbf{V}_2^F$ that is an FFT of the receiver replica signal with a Doppler frequency 500 Hz to test 20 coarse Doppler frequencies at 1 kHz from -4.5 kHz to 4.5 kHz.

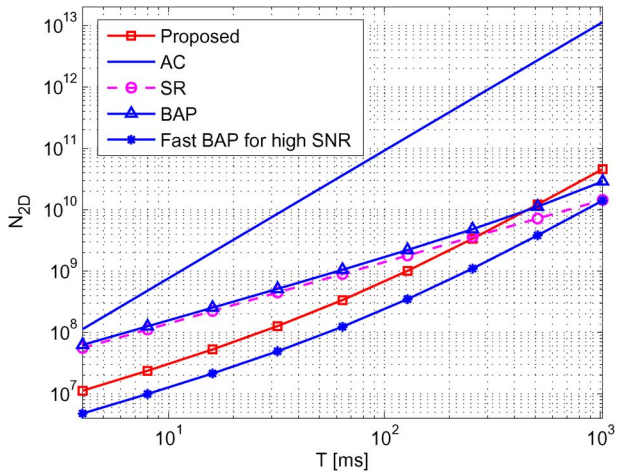

Fig. 4. N_{2D} for a coherent integration.

Fig. 4 shows the total number of complex multiplications N_{2D} for the four techniques performing coherent integrations with the same interval T, as compared in Table I. The fast BAP technique may achieve the highest acquisition speed for strong signals, however, as it suffers from a large SNR loss (more than 10 dB) for weak signals, the effective N_{2D} for the fast BAP technique should be at least 10 times larger T. Note that in Table I, the BAP technique has $\log_2(R_s Q_1)$ term that can be much larger for FFT operation in practice when R_s is not an integer power of 2, which is neglected in Fig. 4. As shown, the proposed technique requires much less computation than the AC technique by 10 to 100 times, and the proposed technique requires a few to several times less computation than the BAP and SR techniques for $T \ll 1$ s.

B. Mean Acquisition Computation

The MAC of the AC, BAP, and proposed techniques is evaluated by 10^5 Monte Carlo simulations for a GPS receiver with $B = 2.046$ MHz and $f_s = q_c R_s R_c$ searching for a C/A code signal with $T = R_T T_1 = R_T$ ms, $q_c = 4$, $R_s = 3$ and $p_v = 10$. In addition, the MAC of the proposed technique is also evaluated based on the MAC expression (57) and the estimated P_D, P_M, P_f, and P_F with measurements of real GPS signals whose signal powers are $C/N_0 \simeq 20, 22, 26, 30$ dB-Hz. In the

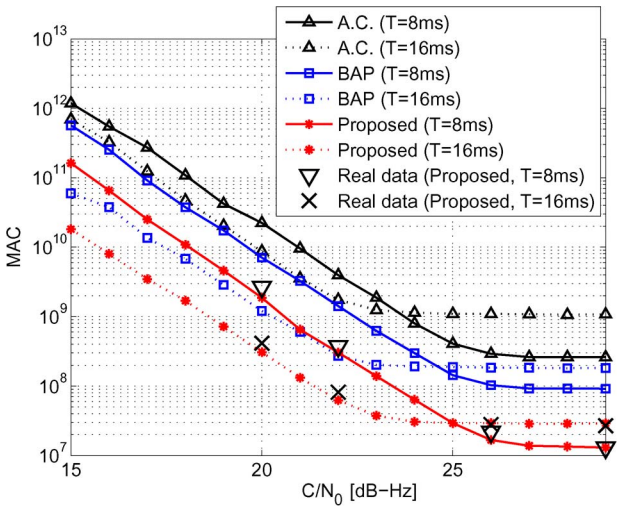

Fig. 5. MAC comparison for a coherent integration.

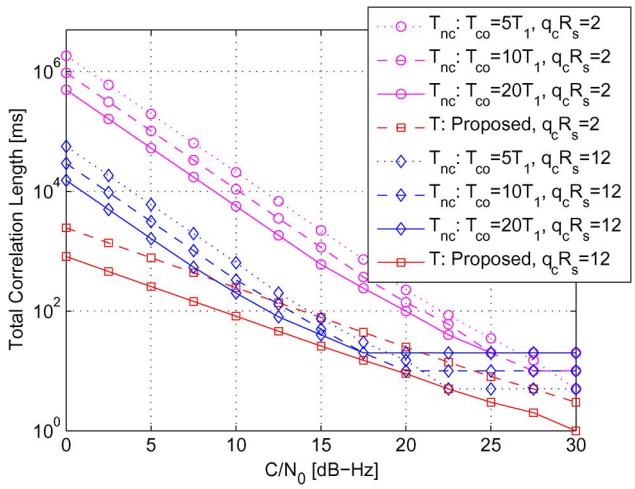

Fig. 6. T vs. T_{nc} to achieve 10 dB target post-RSS SNR.

MAC evaluations shown in Fig. 5, the effect of the navigation data and bit boundary is not considered, i.e., the target signal is a data-free signal and the receiver oscillator is stable during R_T ms. In the simulations, all three techniques use predetermined detection thresholds for CFAR (constant false alarm rate) $P_F = 5 \times 10^{-3}$, and complex multiplication for the FFT of receiver replica signal is not counted, since a receiver may have the FFT'd receiver replica signal stored in a memory. For the proposed technique, $f_m = R_T/2$ and $M_f = 4$ from (18) are used so that there are only 21 sparse Doppler frequencies for the SDFS. In the AC technique, $q_c R_s$ times coherent FFT-based correlations (of length $2R_cT$) are performed to test q_cR_s sample offsets for each Doppler frequency hypothesis; there are $F_m = 161$ and $F_m = 321$ Doppler frequency hypotheses for $T = 8$ ms and $T = 16$ ms, respectively. In the BAP technique, since $R_T = 8$ and 16, we generate 8 and 16 equally spaced Doppler frequencies to test between [0, 500] Hz, which is smaller number than 20 used in [5]. As shown in Fig. 5, the MAC of the proposed technique evaluated from simulations follows the MAC based on real GPS measurement data and is much smaller than those of the AC and BAP techniques. For $T = 8$ ms and $T = 16$ ms, the proposed technique only requires about 20 and 30 times less complexity, respectively, than the AC technique for all C/N$_0$, and requires about 5 and 3 times less complexity, respectively, than the BAP technique for all C/N$_0$. Note that when the signal is strong enough, it is expected from Fig. 5 that the MAC is about the half of N_{2D} shown in Fig. 4. Note also that considering the results in Fig. 4, the performance of the SR technique is expected to have couple of times larger MAC than the proposed technique.

The analysis of the MAT (53) and MAC (58) in this paper is for AWGN channels, and in the presence of strong multipath carrier phase distortion in the received signal may appear and the performance degradation can be expected. However, since the proposed technique requires much smaller MAT and MAC than other coherent integration techniques, the proposed technique suffers much less from strong multipath signals.

C. Complexity Comparison to Non-Coherent Techniques

The simulation results in Fig. 4 and Fig. 5 and the algebraic expressions in Table I are for coherent integrations. However, for a weak GPS signal detection, non-coherent accumulation of multiple coherent integration results is a widely used technique in practice for receivers to avoid the negative impact of bit transition. However, when the target signal is weak, a coherent integration over a small interval T_{co} shorter than the bit width ($T_{co} > T_b$) may results in a very small or even negative coherent SNR, and there may be a negative impact of squaring loss on the final post-RSS (root-sum-of-squares) SNR [9]. As a result, the number of non-coherent accumulations N_{nc} should be much larger than $R_{T_{co}} = T/T_{co}$ to compensate the SNR degradation. Fig. 6 shows the total correlation length T of the proposed technique and $T_{nc} = N_{nc}T_{co}$ of non-coherent integration techniques to achieve 10 dB post-RSS SNR for three T_{co} values $5T_1$, $10T_1$, and $20T_1$ and for two sampling rates $q_cR_s = 2$ and $q_cR_s = 12$, where $q_cR_s = 2$ represents a normal sampling rate $f_s = 2R_c$. As expected, the coherent integration using the proposed technique requires much smaller total correlation length T than T_{nc} in all cases. For an example with the AC technique, when C/N$_0$ = 5dB-Hz, $T_{co} = 10$ ms, 2.046 MHz pre-correlation bandwidth, and $q_cR_s = 12$ are assumed, the expected coherent SNR (before squaring) is -7 dB (=5 dB-Hz $-$ 63 dB $+$ 51 dB) and the squaring loss is about -7 dB [9], which results in -14 dB post-RSS SNR so that the additional gain of 24 dB from N_{nc} should be obtained to achieve the target post-RSS SNR (10 dB). Notice that $N_{nc} \simeq 250$ (equivalently, $T_{nc} = 2500$ ms) achieves the additional 24 dB as shown.

Fig. 7 compares N_{2D} required to achieve 10 dB post-RSS SNR for the proposed, AC, and SR techniques for weak GPS $L1$ C/A code signals (i.e., 0 dB-Hz $\leq$ C/N$_0$ $\leq$ 30 dB-Hz). In the simulations, it is assumed that the navigation data bit boundary is aligned with the boundary of T_{co} for a simplicity and that $q_cR_s = 12$, and $T_{co} = 5T_1$, $10T_1$, and $20T_1$ are tested. As shown, the proposed technique has much (from a few to about hundred times) smaller N_{2D} than the AC and SR techniques for almost all C/N_0 values.

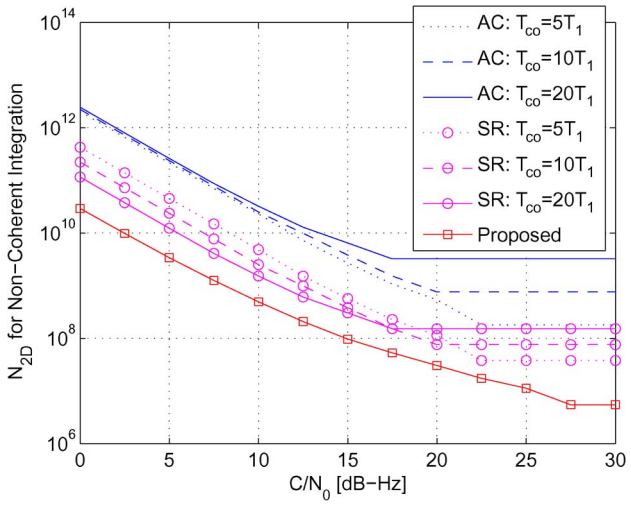

Fig. 7. N_{2D} to achieve 10 dB target post-RSS SNR.

VII. Conclusion

A low computational long coherent integration technique based on SDFS and SDHT has been proposed in this paper. It has been found that, using the proposed SDFS and SDHT, a number of Doppler frequency hypothesis tests can be performed without actual correlations between the incoming signal and the receiver replica signal. As a result, it has been demonstrated that the proposed SDFS and SDHT technique can reduce the computational complexity of the acquisition of severely attenuated GNSS signals significantly. The performance of the proposed technique has been numerically evaluated, demonstrated with real GPS measurements, and the numerous Monte Carlo simulation results have shown a good match to the theoretical performance estimates. From numerical simulations, it has been shown that the proposed technique requires multiple times less complex multiplications than the conventional techniques, and that the computational advantage of the proposed technique increases as the strength of the received signal decreases.

Appendix A

The P_F, P_f, and probabilities of detection and miss are

$$P_F = 1 - \left[1 - \exp\left(\frac{-\gamma}{V_0}\right)\right]^{q_1} \tag{59a}$$

$$P_f = \left[1 - \left[1 - \exp\left(\frac{-\gamma}{V_0}\right)\right]^{q_1-1}\right] \times \left[1 - \sum_{k=0}^{q_1-1} \binom{q_1-1}{k} \frac{(-1)^k}{1+k} \exp\left(\frac{-kZ}{(1+k)V_0}\right)\right] \tag{59b}$$

$$P_D = Q\left(\sqrt{\frac{2Z}{V_0}}, \sqrt{\frac{2\gamma}{V_0}}\right) \times \left[\sum_{k=0}^{q_1-1} (-1)^k \binom{q_1-1}{k} \frac{1}{1+k} \exp\left(\frac{-kZ}{(1+k)V_0}\right)\right] \tag{59c}$$

$$P_M = 1 - P_D - P_f \tag{59d}$$

TABLE II
Key Variables and Definitions

Variable	Definition
f_s	sampling rate
f_m	maximum allowed Doppler frequency offset ($f_m = R_T/2$)
F_m	number of total Doppler frequency hypotheses to be searched for a coherent integration interval T
M_f	maximum offset factor ($M_f = 4$)
L_c	code length of the spreading sequence
L'_c	smallest integer power of $2 \geq L_c$
N_{nc}	number of non-coherent accumulations
T_1	short partial coherent integration interval ($T_1 = 1$ms)
T	long coherent integration interval
T_{co}	coherent integration interval used for the non-coherent integration scheme
T_{nc}	overall integration interval of the non-coherent integration scheme
R_T	T/T_1
$R_{T_{co}}$	T/T_{co}
R_c	chip rate
R_s	sample compression rate per chip ($R_s = f_s/(q_c R_c)$)
q_c	number of compressed samples per chip ($q_c \geq 2$)
q_1	number of compressed samples within T_1 ($q_1 = f_s T_1/R_s = q_c L_c$)
Q_1	smallest integer power of $2 \geq 2q_1$ ($Q_1 = 2q_c L'_c \simeq 2q_c L_c \simeq 2q_1$ in this paper)

respectively, where $Q(a, b)$ is the Marcum's Q-function [20]

$$Q(a,b) = \int_b^\infty x \exp\left(\frac{-(x^2+a^2)}{2}\right) I_0(ax)\, dx. \tag{60}$$

Appendix B

Since there are F_m Doppler frequency hypotheses to test for the conventional parallel search techniques, the overall branch transfer function of the conventional parallel search technique is

$$H(T) = \frac{H_D(T)[1 - H_0^{F_m}(T)]}{F_m[1 - H_0(T)][1 - H_M(T)H_0^{F_m-1}(T)]}, \tag{61}$$

where the correct hypothesis detection, correct hypothesis missed, and incorrect hypothesis branch transfer functions are found as

$$H_D(T) = P_D T^{p_v+1} + (1 - P_F)T + (1 - P_f)T \tag{62a}$$

$$H_M(T) = P_M T + P_f T^{p_v+1} \tag{62b}$$

$$H_0(T) = (1 - P_F)T + P_F T^{p_v+1}, \tag{62c}$$

respectively, and T^{p_v} is the penalty time for verification [18].

Appendix C

Table II lists the key variables with definitions.

REFERENCES

[1] B. Parkinson, J. Spilker, P. Axelrad, and P. Enge, Eds., *Gobal Positioning System: Theory and Applications*. Washington, DC, USA: American Institute of Aeronautics and Astronautics, 1996.

[2] K. Borre, D. M. Akos, N. Bertelsen, P. Rinder, and S. H. Jensen, *A Software-Defined GPS and Galileo Receiver: A Single-Frequency Approach*. Cambridge, MA, USA: Birkhäuser, 2007.

[3] J. A. Starzyk and Z. Zhu, "Averaging correlation for C/A code acquisition and tracking in frequency domain," in *Proc. 44th IEEE MWSCAS*, Aug. 14–17, 2001, vol. 2, pp. 905–908.

[4] D. Akopian,"Fast FFT based GPS satellite acquisition methods," *Proc. Inst. Elect. Eng.—Radar, Sonar Navig.*, vol. 152, no. 4, pp. 277–286, Aug. 2005.

[5] M. Sahmoudi, M. G. Amin, and R. Landry, Jr., "Acquisition of weak GNSS signals using a new block averaging pre-processing," in *Proc. IEEE/ION PLANS*, May 6–8, 2008, pp. 1362–1372.

[6] C. Yang, J. Vasquez, and J. Chaffee, "Fast direct P(Y)-code acquisition using XFAST," in *Proc. 12th ITM Satell. Div. ION GPS*, Nashville, TN, USA, Sep. 1999, pp. 317–324.

[7] H. Li, X. Cui, M. Lu, and Z. Feng, "Dual-folding based rapid search method for long PN-code acquisition," *IEEE Trans. Wireless Commun.*, vol. 7, no. 12, pp. 5286–5296, Dec. 2008.

[8] S.-H. Kong and B. Kim, "Two-dimensional compressed correlator for fast PN acquisition," *IEEE Trans. Wireless Commun.*, vol. 12, no. 11, pp. 5859–5867, Nov. 2013.

[9] F. Van Diggelen, *A-GPS: Assisted GPS, GNSS, and SBAS*. Norwood, MA, USA: Artech House, 2009.

[10] N. F. Kransner, "GPS receiver and method for processing GPS signals," U.S. Patent PN 5 781 156, Jul. 14, 1998.

[11] T. Pany *et al.*, "Coherent integration time: The longer, the better," *Inside GNSS*, pp. 52–61, Nov./Dec. 2009.

[12] S. H. Kong, "Fast multi-satellite ML acquisition for A-GPS," *IEEE Trans. Wireless Commun.*, vol. 13, no. 9, pp. 4935–4946, Sep. 2014.

[13] M. L. Psiaki, "Block acquisition of weak GPS signals in a software receiver," in *Proc. ION GPS Conf.*, Salt Lake City, UT, USA, Sep. 2001, pp. 1–13.

[14] A. J. Viterbi, *CDMA: Principles of Spread Spectrum Communication*. Reading, MA, USA: Addison-Wesley, 1995.

[15] B. Kim and S.-H Kong, "Determination of detection parameters on TDCC performance," *IEEE Trans. Wireless Commun.*, vol. 13, no. 5, pp. 2431–2422, May 2014.

[16] A. Papoulis, *Probabilities and Random Variables*. Englewood Cliffs, NJ, USA: Prentice-Hall, 1990.

[17] G. E. Corazza, "On the MAX/TC criterion for code acquisition and its application to DS-SSMA systems," *IEEE Trans. Wireless Commun.*, vol. 44, no. 9, pp. 1173–1182, Sep. 1996.

[18] P. W. Ward, "GPS receiver search techniques," in *Proc. IEEE PLANS*, Atlanta, GA, USA, Apr. 1996, pp. 604–611.

[19] C. Yang, "FFT acquisition of periodic, aperiodic, puncture, and overlaid code sequences in GPS," in *Proc. 14th ITM Satell. Div. ION GPS*, Salt Lake City, UT, USA, Sep. 2001, pp. 137–147.

[20] J. I. Marcum, "A table of Q-functions," Rand Corp., Santa Monica, CA, USA, Rep. RM-339, Jan. 1950.

Seung-Hyun Kong (M'06) received the B.S. degree in electronics engineering from the Sogang University, Korea, in 1992, the M.S. degree in Electrical Engineering from the Polytechnic University, New York, USA, in 1994, and the Ph.D. degree in Aeronautics and Astronautics from Stanford University, Stanford, CA, USA, in 2006. From 1997 to 2004, he was with Samsung Electronics Inc. and Nexpilot Inc., both in Korea, where his research focus was on wireless communication systems and UMTS mobile positioning technologies. In 2006, he was involved with hybrid positioning technology development using wireless location signature and Assisted GNSS at Polaris Wireless, Inc., Santa Clara, CA, and from 2007 to 2009, he was a research staff at the Corporate R&D of Qualcomm Inc., San Diego, CA, where his R&D focus was on the indoor location technologies and advanced GNSS technologies. Since 2010, he is an Associate Professor at the Korea Advanced Institute of Science and Technology (KAIST). His research interests include next generation GNSS, advanced signal processing for navigation systems, and vehicular communication systems.